Iranian Society of Acoustics and Vibration
The 14th ISAV2024 International Conference on Acoustics and Vibration
11-12 Dec 2024 Karaj - Iran
Kharazmi University

Design and Simulation of Acoustic Metamaterial Luneburg Lenses for Predetermined Focal Points

Mohammad Naeim Moradi[a], Abdolreza Ohadi[b*], Maryam Ghassabzadeh Saryazdi[c]

[a] *PhD student, Acoustics Research Laboratory, Mechanical Engineering Department, Amirkabir University of Technology (Tehran Polytechnic), Tehran, Iran.*

[b] *Professor, Acoustics Research Laboratory, Mechanical Engineering Department, Amirkabir University of Technology (Tehran Polytechnic), Tehran, Iran.*

[c] *Assistant Professor, Vehicle Technology Research Institute, Amirkabir University of Technology (Tehran Polytechnic), Tehran, Iran.*

** Corresponding author e-mail: a_r_ohadi@aut.ac.ir*

Abstract

The design and simulation of acoustic metamaterial lenses for focusing elastic waves at predetermined focal points are presented in this article. Based on modified Luneburg refractive index profiles, three distinct lenses are designed, each to target specific focal points. A key contribution is the proposal of hexagonal unit cells containing blind holes with varying diameters. Finite element simulations are conducted to obtain dispersion curves, determining each unit cell's wave properties, including the refractive index. These unit cells provide a wide range of refractive indices from 1.0314 to 1.4959 at the design frequency of 50 *kHz* which is suitable for constructing the desired lenses. Unit cells are then arranged according the aforementioned discretized profiles to shape the required lenses. Numerical simulations validate effective elastic wave focusing at the intended focal points (*F=R, 1.5R, 2R*) with three lenses. The strongest wave concentration occurs at focal points closer to the lens, with the design for *F=R* achieving the highest level of focusing based on maximum velocity values. As the focal point shifts from *R* to *2R*, the wave distribution becomes scattered along the focal axis, which is believed to be appropriate for acoustic/elastic jet applications. This study demonstrates the potential of these lenses in precisely controlling acoustic/elastic wave propagation, which has significant applications in enhancing resolution and accuracy for non-destructive testing, industrial imaging, and optimizing energy harvesting.

Keywords: Acoustic Metamaterials; Luneburg lens; Predetermined Focal Points; Elastic Waves.

1. Introduction

In recent years, there has been growing interest in the field of acoustic metamaterials (AMs). AMs are artificial materials that can control sound waves through innovative mechanisms like local resonances or geometrical arrangements, often achieving unnatural effects like negative refraction. Acoustic metamaterials have potential applications in various industrial and medical fields[1–3] as acoustic absorbers[4,5], barriers[6], lenses[7–9] and cloaks[10]. Acoustic lenses are mainly devices that are specifically designed to focus sound waves in one or multiple focal points. The unique properties of lenses are useful for applications like sensing and damage detection in solids[11], non-destructive testing[12], and energy harvesting[13].

The literature surrounding acoustic metamaterial lenses highlights various approaches to wave focusing, with different geometries and working mechanisms. Zhao et al. [14] in their 2023 study, introduced a structural Luneburg lens for broadband ultralong subwavelength focusing, utilizing two concentric circular regions with varying thickness in a thin plate to achieve double foci and control energy flow between the two focal spots. In a related study at 2022, Zhao et al. [15] explored the Rays Inserting Method (RIM), to design acoustic lenses for flexural wave manipulation by varying the thickness of thin plates to achieve a desired refractive index profile. Similarly, Climente et al. [16] developed gradient-index lenses with one focal point for flexural waves based on the thickness-dependence of the dispersion relation, designing five distinct lenses using local thickness variations in thin plates to guide wave propagation. Wu et al. [17] focused the lowest anti-symmetric Lamb wave in gradient-index phononic crystal (PC) plates, demonstrating lens's application as a beam-width compressor for Lamb waves in a silicon waveguide. Tol et al. [18] designed a gradient index lens for elastic wave energy harvesting, using an array of blind holes with varying diameters in an aluminium plate, though their lens lacked omnidirectionality and used square unit cells. Building on this in the year 2017, Tol et al. [13] developed a phononic crystal Luneburg lens with omnidirectional elastic wave focusing, though without control over the focal point. Additionally, Zhao et al. [19] studied the beam paths and focusing behaviour of high-frequency flexural Lamb waves in acoustic lenses, achieving sub-wavelength focusing in perforated plates.

In contrast to previous studies, this paper presents a lens design based on hexagonal unit cell with blind holes, which offers greater structural integrity compared to fully perforated and variable thickness designs, while bringing in the ability to approximate modified Luneburg lens profiles. This unit cell design is in such a way that it provides desired acoustic properties (refractive index of the unit cell) by adjusting the diameter of blind holes. It offers a wide range of refractive indices at the design frequency of 50 *kHz* which is not common among previous researches. The main objective of this paper is to achieve arbitrary focal points with different variants of the proposed structure which is crucial for precise wave control in real-world applications of the lens. For this reason, three distinct lenses are designed. Their performance is validated through finite element simulations in COMSOL. In the subsequent sections, section 2 comprehensively explains the procedure for lens design, section 3 covers the finite element simulations, presenting the results and analysing them in detail. Lastly, Section 4 concludes the paper, summarizing the key findings from the study.

2. Lens Design Principles

Among acoustic lenses, gradient refractive index lenses (GRIN) have the property of spatially variable refractive index within the metamaterial and therefore easily manipulating the incident waves. Luneburg lens (originally in optics) is a symmetric gradient-index lens that can focus acoustic waves from any direction to an arbitrary point and thus is chosen as a suitable lens for this study[20]. The governing equation of the modified acoustic Luneburg lens[9] presents the refractive index $n(r)$ at any point within the Luneburg lens as a function of the radial distance r from the center of the lens[9]:

$$n(r) = \frac{\sqrt{F^2 + R^2 - r^2}}{F} \qquad (1)$$

where R is the radius of the lens and F is the location of the focal point. The traditional profile of Luneburg lens can be achieved by using $F=R$ in Eq. (1). Based on this governing equation which is shown in Figure 1 for three cases of $F = R$, $1.5R$, $2R$, the refractive index is highest at the center of the lens and decreases radially toward the edge. Low refractive index in outer boundaries results in impedance matching with background medium. Also, the smooth transition of refractive index allows sound waves to travel along curved paths within the lens. Therefore, the acoustic waves can enter and travel within the lens without any reflection.

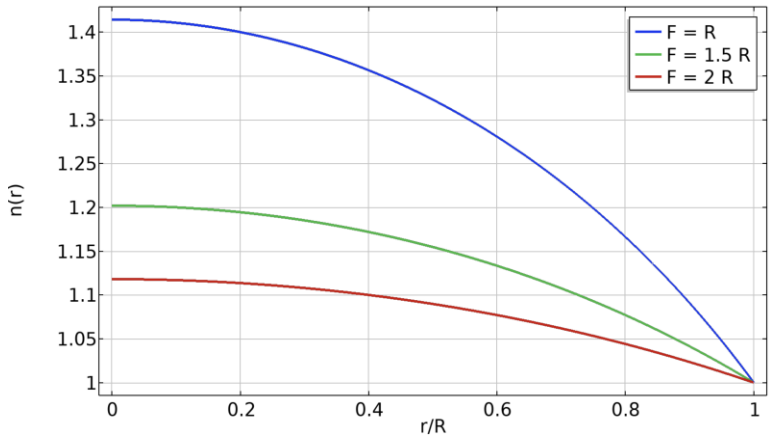

Figure 1. Refractive index profile of modified Luneburg lenses.

To create a practical Luneburg lens, a unit cell able to create spatially varying refractive index should be proposed. For this reason, many concepts have been introduced by means of material or size variations. Examples include periodically arranged cross shape cells[9], perforated plates with different hole sizes[19], and variable thickness plates[16]. As demonstrated by Figure 2.a, hexagonal unit cells with blind holes of various diameters in the middle are proposed in this study. This choice results in a hexagonal final shape of the lens (Figure 2.b) which is a close shape to a circular Luneburg lens. The use of a blind hole design, rather than a basic perforated plate, enhances the structural integrity of the lens.

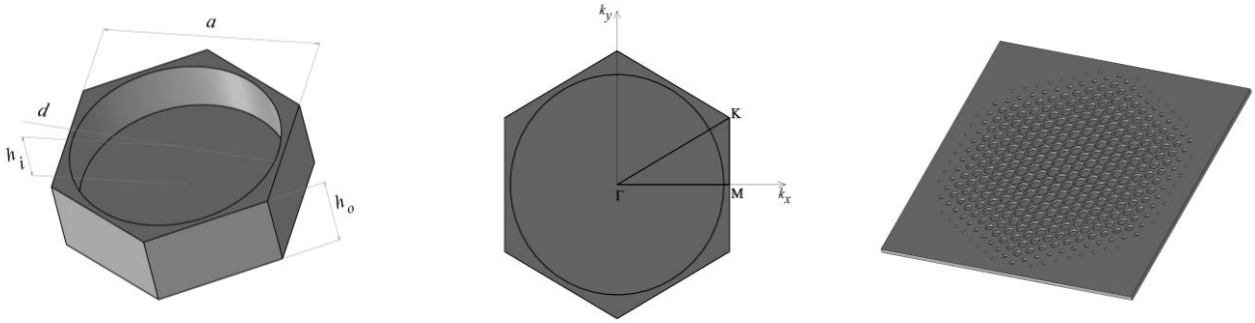

a b c

Figure 2. a) Hexagonal unit cell. **b)** Irreducible Brillouin zone. **c)** Luneburg lens based on refractive index profile with $F=R$.

The refractive indices of unit cells should be calculated to then properly arrange the cells next to each other and form the complete lens. This is done by deriving dispersion curves, which provide insight into how waves propagate through the periodic structure at different frequencies. Calculating the dispersion curves involves solving the eigenvalue problem derived from the Floquet-Bloch theorem applied to the wave equation in solids. The wave equation for elastic wave propagation in a solid is given by[21]:

$$\nabla.(C:\nabla u)=\rho\frac{\partial^2 u}{\partial t^2} \qquad (2)$$

where C is the stiffness tensor, u is the displacement vector, and ρ is the density of the material. According to the Floquet-Bloch theorem, the solution to the wave equation in a periodic structure can be expressed as[22]:

$$u(r)=u_p(r)e^{ik.r} \quad (3)$$

where $u_p(r)$ is a periodic function with the same periodicity as the crystal structure, and $e^{ik.r}$ is a phase factor representing the wavevector k. Substituting this form into the wave equation with periodic coefficients results in an eigenvalue problem, which is solved to obtain the dispersion relation $\omega=\omega(k)$. The computation of the dispersion relation is performed within the first Brillouin zone, which is the fundamental region in reciprocal (k_x-k_y) space for periodic structures. Due to the symmetry of the crystal, it is sufficient to compute the dispersion relation within the irreducible part of the Brillouin zone, rather than the entire lattice, which significantly reduces computational effort. This zone has all the unique wave propagation behavior of the structure, making it possible to predict wave behavior across the entire periodic medium.

The dispersion curves are calculated (shown and verified in Figure 3) using finite element method (FEM) simulations in COMSOL Multiphysics, where the eigenvalue problem is solved numerically over the irreducible Brillouin zone (IBZ). The IBZ is determined as shown in Figure 2.c. Floquet-Bloch periodicity is applied to the sides of the unit cell. Then by parametric sweeping of the wave vector k_x from *0* to π/a, eigenfrequencies are computed at each wavenumber value and the dispersion diagram is formed. For a design frequency of 50 *kHz*, the hexagonal unit cell is considered with constant dimensions of $a = 8\ mm$, $h_o = 3.175\ mm$, and $h_i = 2.175\ mm$. However, diameter of the blind hole is considered as design parameter and is changed to achieve a desirable refractive index from the cell.

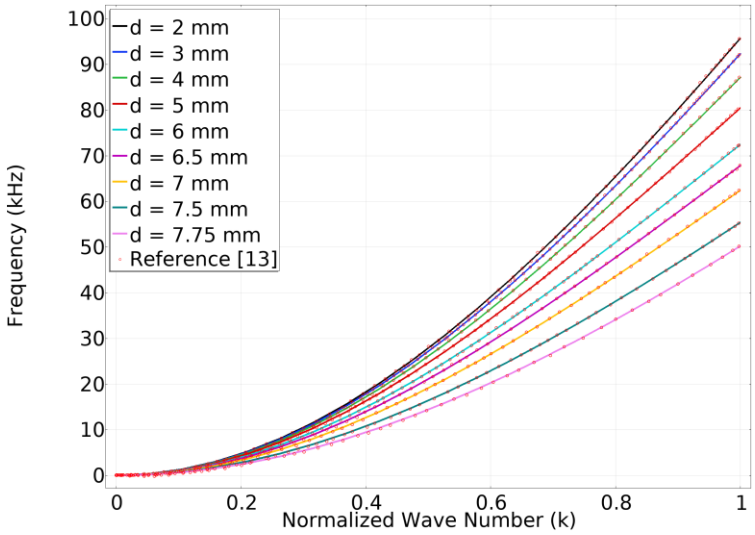

Figure 3. Dispersion diagram of unit cells of different diameter blind hole.

By examining the relationship between the wave vector and frequency (dispersion relation), the material's dispersion properties like wave propagation speed can be determined. The refractive index can then be calculated using Eq. (4) as follows[13]:

$$n=\frac{c}{c_{\Gamma M}} \quad (4)$$

in which $c_{\Gamma M}$ is the phase velocity in the ΓM direction of the unit cell and c is the reference phase velocity of the first antisymmetric mode wave in a homogenous aluminium plate of the same thickness as the lens. The first antisymmetric mode represents the fundamental mode of wave propagation at design frequency of this paper. The refractive indices of various unit cells are computed and

reported in Table 1. This table indicates a broad range of refractive indices, from 1.03 to 1.4959, achievable at the design frequency with the proposed unit cells of different blind hole diameters. This wide range is particularly appropriate, because it allows for the precise design of modified Luneburg lens profiles through careful arrangements of unit cells next to each other in multiple concentric layers.

Table 1. Refractive index of unit cells of different hole diameters at design frequency of 50 *kHz*.

Diameter (mm)	Refractive Index
2	1.0314
3	1.0492
4	1.0768
5	1.1185
6	1.1853
6.5	1.2360
7	1.3051
7.5	1.4096
7.75	1.4959

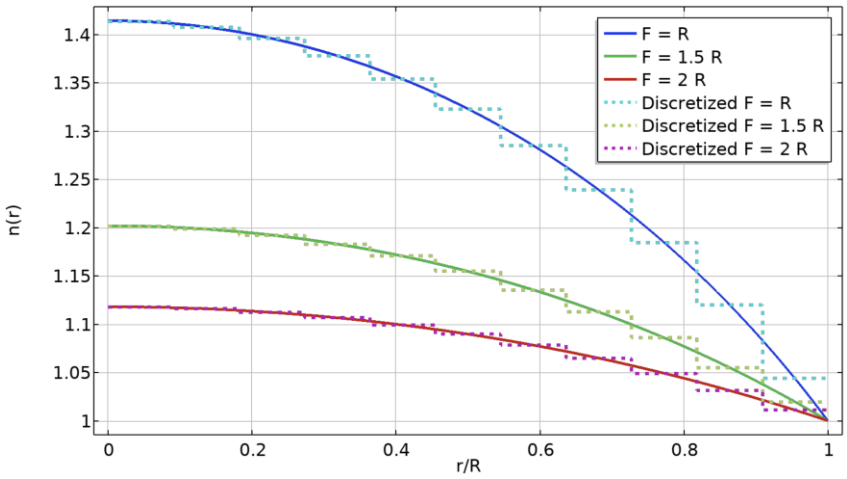

Figure 4. Discretized Refractive index profile of Luneburg lens.

Based on the governing equation of the modified Luneburg lens, three hexagonal lenses are designed for three different focal points (*F=R, 1.5R, 2R*). One of the lenses (*F = R*) is shown in Figure 2.c. The three aforementioned modified Luneburg lens profiles are discretized to 11 layers as shown in Figure 4. The arrangement of the unit cells next to each other in concentric layers is based on refractive index of each unit cell and the required position of that refractive index in the profile.

Table 2. Blind hole diameters (mm) in each layer for three designed lenses.

Layers	*F = R*	*F = 1.5R*	*F = 2R*
1	7.5	6.25	5
2	7.5	6.25	5
3	7.5	6	5
4	7.25	6	4.75
5	7.25	5.75	4.75
6	7	7.5	4.5
7	7	5.25	4
8	6.5	5	3.5
9	6	4	3
10	5	3	2
11	3	2	2

The unit cells with largest blind holes are located around the center of the lens and small holes are located toward the edge of the lens. All three lenses have a diameter of 176 *mm* (R = 88 *mm*) consisting of 379 unit cells in 11 layers. Table 2 includes the corresponding diameters of blind holes in each layer of the three lenses.

3. Simulations and Results

Evaluating the lens performance in focusing elastic waves is done by means of finite element simulations in COMSOL Multiphysics software. The solid mechanics module is employed to perform a structural analysis in the frequency domain, allowing for derivation of the instantaneous displacement, velocity, and stress fields without the need for a time-dependent study. Frequency domain study (at design frequency of 50 *kHz*) is specifically used to compute the response of the wave equation in solids to a harmonic wave with respect to particular load distributions. This provides the displacement field (u). The velocity field can then be derived directly by applying the relation $v=i\omega u$, where v is the velocity field, ω is the angular frequency.

Simulation domain is chosen as a plate of 800×300 mm^2 area for $F = R$, a plate of 1000×300 mm^2 area for $F = 1.5R$ and a plate of 1200×300 mm^2 area for $F = 2R$ with a thickness of 3 *mm* in all cases. Aluminium with constants of elasticity E = 70 *GPa*, density ρ = 2700 kg/m^3 and Poisson's ratio of ν = 0.33 is considered as the material for this study. Boundary load of F_z = 1 *N* is applied to the left side of the plate and other sides are considered as low reflection boundary. Mesh size is set to be 7 mesh elements per wavelength in the design frequency of 50 *kHz*.

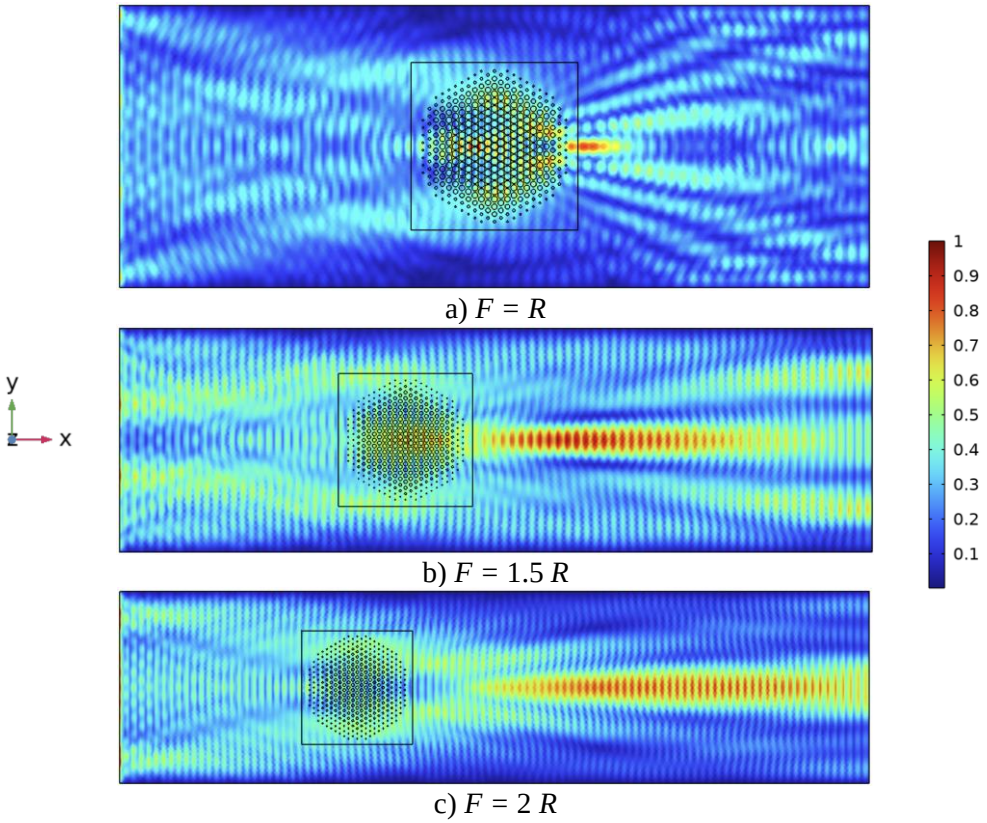

a) $F = R$

b) $F = 1.5\ R$

c) $F = 2\ R$

Figure 5. Normalized rms instantaneous velocity fields in simulation domain[1].

The normalized rms instantaneous velocity fields of Figure 5 are obtained as a result to verify the findings of this study. As shown by this figure elastic wave focusing is obtained by the proposed

[1] *Scales in Figure 5 are set to a) 1:8 b) 1:10 c) 1:12.*

lenses of this study at three different focal points. In all three cases the waves are curved toward the focal point of the lens, confirming the lens's gradient refractive index profile. It can be observed that wave concentration is stronger at focal points closer to the lens. As the focal point moves from *R* to 2*R*, the focal length increases accordingly. This brings out the possibility of using this type of lens for creating acoustic/elastic wave jets.

Figure 6 illustrates the rms value of velocity over *y* coordinate. The *xyz* coordinate is placed in the middle of the upper surface of the lens with *y* being parallel to width of the domain (y is ranging from -150 to 150 *mm* to cover 300 *mm*). As shown by this graph focusing elastic wave is successfully achieved by the proposed lens at the vicinity of the intended focal points. With an increase in focal point the distribution of waves is being scattered along the *y* axis, and lens with $F = R$ shows the highest level of focusing elastic waves based on the maximum velocity that is reached.

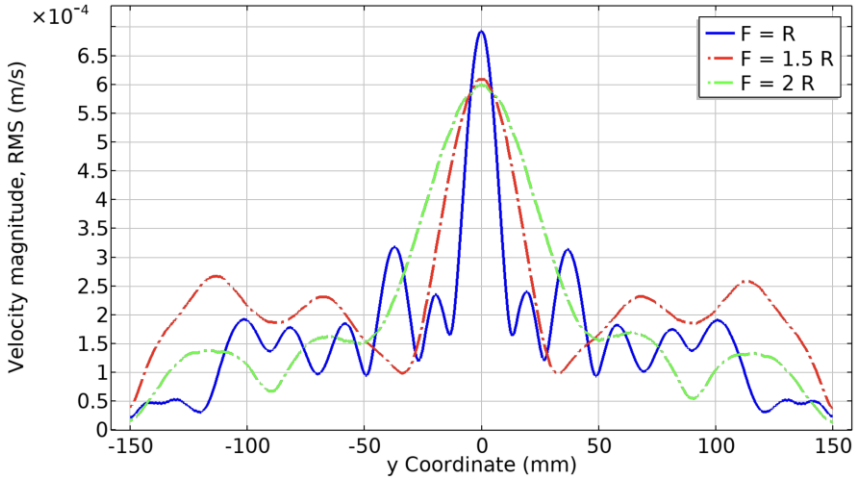

Figure 6. RMS instantaneous velocity over y coordinate.

4. Conclusion

This paper demonstrates the design and simulation of three lenses for focusing elastic waves at three different focal points using acoustic metamaterial Luneburg lens concept. The hexagonal unit cells presented in this study have design parameters which enables them to achieve a wide range of refractive indices, ranging from 1.0314 to 1.4959 at the design frequency of 50 kHz. Dispersion curves are calculated via finite element method simulations, and as a result the refractive index is derived for each unit cell at the design frequency of 50 kHz. The lenses are formed by arranging hexagonal unit cells with blind holes of varying hole diameters based on modified Luneburg lens refractive index profiles. The results from numerical wave simulations confirmed the accurate focusing of waves at the intended focal points of $F = R$, $1.5R$, and $2R$, validating the effectiveness of the design. The lens designed for $F = R$ achieved the highest level of focusing based on maximum velocity values. As the focal point shifted from *R* to *2R*, the wave distribution became scattered along the focal axis. The adaptability and structural integrity of the proposed design make this approach a promising path for advanced wave manipulation. The results of this study offer significant potential for applications in areas such as industrial non-destructive testing, imaging, and energy harvesting.

REFERENCES

[1] M.H. Lu, L. Feng, Y.F. Chen, Phononic crystals and acoustic metamaterials, Mater. Today 12 (2009) 34–42. https://doi.org/10.1016/S1369-7021(09)70315-3.

[2] H. Ge, M. Yang, C. Ma, M.H. Lu, Y.F. Chen, N. Fang, P. Sheng, Breaking the barriers: Advances in

acoustic functional materials, Natl. Sci. Rev. 5 (2018) 159–182. https://doi.org/10.1093/nsr/nwx154.
[3] G. Liao, C. Luan, Z. Wang, J. Liu, X. Yao, J. Fu, Acoustic Metamaterials: A Review of Theories, Structures, Fabrication Approaches, and Applications, Adv. Mater. Technol. 6 (2021) 1–29. https://doi.org/10.1002/admt.202000787.
[4] K. Yu, N.X. Fang, G. Huang, Q. Wang, Magnetoactive Acoustic Metamaterials, Adv. Mater. 30 (2018) 1–10. https://doi.org/10.1002/adma.201706348.
[5] Z. Liang, J. Li, Extreme acoustic metamaterial by coiling up space, Phys. Rev. Lett. 108 (2012) 1–4. https://doi.org/10.1103/PhysRevLett.108.114301.
[6] M. Sun, X. Fang, D. Mao, X. Wang, Y. Li, Broadband Acoustic Ventilation Barriers, Phys. Rev. Appl. 13 (2020) 1. https://doi.org/10.1103/PhysRevApplied.13.044028.
[7] N. Jiménez, V. Romero-García, L.M. García-Raffi, F. Camarena, K. Staliunas, Sharp acoustic vortex focusing by Fresnel-spiral zone plates, Appl. Phys. Lett. 112 (2018). https://doi.org/10.1063/1.5029424.
[8] Y. Zhu, B. Assouar, Multifunctional acoustic metasurface based on an array of Helmholtz resonators, Phys. Rev. B 99 (2019) 174109. https://doi.org/10.1103/PhysRevB.99.174109.
[9] L. Zhao, T. Horiuchi, M. Yu, Broadband acoustic collimation and focusing using reduced aberration acoustic Luneburg lens, J. Appl. Phys. 130 (2021). https://doi.org/10.1063/5.0064571.
[10] Y. Jin, X. Fang, Y. Li, D. Torrent, Engineered Diffraction Gratings for Acoustic Cloaking, Phys. Rev. Appl. 11 (2019) 1. https://doi.org/10.1103/PhysRevApplied.11.011004.
[11] D. Ozevin, S. Tol, Role of acoustic metamaterials and phononic crystals in sensing and damage detection in solids, Elsevier Inc., 2022. https://doi.org/10.1016/B978-0-12-817784-6.00014-X.
[12] H. Selim, R. Picó, J. Trull, M.D. Prieto, C. Cojocaru, Directional ultrasound source for solid materials inspection: Diffraction management in a metallic phononic crystal, Sensors (Switzerland) 20 (2020) 1–18. https://doi.org/10.3390/s20216148.
[13] S. Tol, F.L. Degertekin, A. Erturk, Phononic crystal Luneburg lens for omnidirectional elastic wave focusing and energy harvesting, Appl. Phys. Lett. 111 (2017) 1–6. https://doi.org/10.1063/1.4991684.
[14] L. Zhao, H. Kim, M. Yu, Structural Luneburg lens for broadband ultralong subwavelength focusing, Mech. Syst. Signal Process. 182 (2023) 109561. https://doi.org/10.1016/j.ymssp.2022.109561.
[15] L. Zhao, C. Bi, M. Yu, Acoustic Lenses Design based on the Rays Inserting Method, (n.d.) 1–14.
[16] A. Climente, D. Torrent, J. Sánchez-Dehesa, Gradient index lenses for flexural waves based on thickness variations, Appl. Phys. Lett. 105 (2014). https://doi.org/10.1063/1.4893153.
[17] T.T. Wu, Y.T. Chen, J.H. Sun, S.C.S. Lin, T.J. Huang, Focusing of the lowest antisymmetric Lamb wave in a gradient-index phononic crystal plate, Appl. Phys. Lett. 98 (2011) 2009–2012. https://doi.org/10.1063/1.3583660.
[18] S. Tol, F.L. Degertekin, A. Erturk, Gradient-index phononic crystal lens-based enhancement of elastic wave energy harvesting, Appl. Phys. Lett. 109 (2016). https://doi.org/10.1063/1.4960792.
[19] J. Zhao, B. Bonello, O. Boyko, Beam paths of flexural Lamb waves at high frequency in the first band within phononic crystal-based acoustic lenses, AIP Adv. 4 (2014). https://doi.org/10.1063/1.4905436.
[20] L. Zhao, C. Bi, H. Huang, Q. Liu, Z. Tian, A review of acoustic Luneburg lens: Physics and applications, Mech. Syst. Signal Process. 199 (2023) 110468. https://doi.org/10.1016/j.ymssp.2023.110468.
[21] W.S. Gan, New acoustics, based on metamaterial, 2012. https://doi.org/10.1121/1.4764497.
[22] G. Yi, B.D. Youn, A comprehensive survey on topology optimization of phononic crystals, Struct. Multidiscip. Optim. 54 (2016) 1315–1344. https://doi.org/10.1007/s00158-016-1520-4.